Is the bulk mode conversion important in high density helicon plasma?

Shogo Isayama, Tohru Hada, Shunjiro Shinohara, and Takao Tanikawa

Citation: Physics of Plasmas **23**, 063513 (2016); doi: 10.1063/1.4951017
View online: http://dx.doi.org/10.1063/1.4951017
View Table of Contents: http://scitation.aip.org/content/aip/journal/pop/23/6?ver=pdfcov
Published by the AIP Publishing

Is the bulk mode conversion important in high density helicon plasma?

Shogo Isayama,[1] Tohru Hada,[1] Shunjiro Shinohara,[2] and Takao Tanikawa[3]
[1]*Interdisciplinary Graduate School of Engineering Sciences, Kyushu University, 6-1 Kasuga-Kohen, Kasuga, Fukuoka 816-8580, Japan*
[2]*Institute of Engineering, Tokyo University of Agriculture and Technology, 2-24-16, Naka-cho, Koganei, Tokyo 184-8588, Japan*
[3]*Research Institute of Science and Technology, Tokai University 4-1-1 Kitakaname, Hiratsuka, Kanagawa 259-1292, Japan*

(Received 15 January 2016; accepted 9 May 2016; published online 15 June 2016)

In a high-density helicon plasma production process, a contribution of Trivelpiece-Gould (TG) wave for surface power deposition is widely accepted. The TG wave can be excited either due to an abrupt density gradient near the plasma edge (surface conversion) or due to linear mode conversion from the helicon wave in a density gradient in the bulk region (bulk mode conversion). By numerically solving the boundary value problem of linear coupling between the helicon and the TG waves in a background with density gradient, we show that the efficiency of the bulk mode conversion strongly depends on the dissipation included in the plasma, and the bulk mode conversion is important when the dissipation is small. Also, by performing FDTD simulation, we show the time evolution of energy flux associated with the helicon and the TG waves. [http://dx.doi.org/10.1063/1.4951017]

I. INTRODUCTION

Helicon plasma is a high-density and low-temperature plasma generated by the electromagnetic (helicon) wave excited in a plasma. Since it can be operated in a wide range of external parameters, it is useful for various applications such as plasma processing, electric thrusters, and fundamental plasma research.[1] However, the mechanism of helicon plasma production has been a controversial issue for many years, and it has been studied by many authors theoretically and by laboratory experiments. In 1991, a highly efficient damping of the helicon waves was reported by Chen,[2] suggesting that Landau damping could explain the rapid RF energy absorption into ionization events. However, using an energy analyzer that reduces RF fluctuations in plasma potential, Blackwell and Chen[3,4] in 1998 found no evidence of a deviation of the electron distribution from a pure Maxwellian distribution, and thus the Landau damping mechanism was withdrawn. In 1998, Akhiezer suggested the power absorption mechanism by the kinetic parametric decay instability of the helicon pump wave.[5] The phase velocities of the parametrically excited electrostatic waves (an ion acoustic wave and a lower hybrid wave) can be comparable to the electron or the ion thermal speed. Thus, the parametric decay can be a candidate of a strong power absorption mechanism of the helicon wave. Although the experimental evidence of the parametrically excited electrostatic waves was detected,[6,7] a quantitative estimation has not been given yet. Therefore, the contribution of the kinetic power absorption is still under discussion.

In 1994, Shamrai[8] proposed a model based on a linear mode conversion from the weakly damping helicon wave into the strong dissipative Trivelpiece-Gould (TG) wave. There are two mechanisms of the mode conversion:[9] the surface mode conversion arising from a steep density gradient near insulating walls, and the bulk mode conversion that occurs in the bulk plasma near the mode conversion surface (MCS), where the dispersion curves of the helicon and TG waves merge, $Re(k_{\perp \mathrm{H}}) = Re(k_{\perp \mathrm{TG}})$ ($k_\perp$ is the radial wave number and Re stands for the real part). Aliev and Krämer[10] suggest that the densities at which the bulk mode conversion occurs can be reduced considerably for $m \neq 0$ modes when the density gradient is steep. The surface power absorption by the TG wave excited by the surface mode conversion has been studied intensively.[11–14] Comparisons of numerical models including finite electron mass effect (i.e., TG wave) with experimental data show good agreement with experiments.[15–17] The major contribution of the TG wave for the surface power deposition is widely accepted. On the other hand, Arnush and Shamrai argued that the contribution of the bulk mode conversion to the total power deposition is minor.[9,18]

Based on a fluid model, Kim pointed out that in the bulk mode conversion, collisional dissipation plays an important role near the MCS.[19] When the collision is absent, dispersion curves of the helicon and the TG merge at the MCS. Finite dissipation makes the dispersion curves split and the MCS moves slightly toward a higher density region. Kim argued that the helicon wave is dissipated strongly before it can reach the MCS, making the mode conversion practically absent. Kim further argued that the collisional damping rate of the helicon wave near the MCS is large enough to explain the central core heating (i.e., density profile peaked at the center), a typical property of the helicon plasma in laboratories. Kim estimated the damping length of the helicon wave near the MCS using $k_{\perp \mathrm{imag}}$. However, this is misleading since the imaginary part of $k_\perp$ arises both due to the damping and the evanescence.

In this paper, we make a quantitative argument on the contribution of the bulk mode conversion and the surface

mode conversion on the energy deposition of the helicon wave, by numerically solving a fluid set of Hall MHD equations including the electron mass and the collisional effect. In our model, all the four wave modes, i.e., the helicon waves (H±) and the TG (TG±) waves, with two oppositely propagating directions for both, are included. The energy fluxes associated with these waves are numerically evaluated.

We show that, although the bulk mode conversion takes place anywhere as long as there exists a density gradient in background plasma parameters, the dissipation strongly suppresses the efficiency of the bulk mode conversion due to the separation of the dispersion branches. Our argument is quite different from that of Kims in that the bulk mode conversion occurs even if the helicon and the TG do not merge at the MCS. Note that there is a substantial contribution of the bulk mode conversion to that of the surface mode conversion for power depositions when the collision frequency is small, if the neutral pressure is low, or a neutral depletion occurs.[20–22] Therefore, this paper presents the first report on the contribution fraction of the bulk mode conversion in contrast to the surface one as a function of the collision frequency. By evaluating power depositions of the helicon and the TG waves, we also confirm the importance of the bulk heating near the MCS by the helicon wave as pointed out by Kim. Our results provide the first study on the contributions of power depositions and their profiles of the helicon and the TG waves when the collision frequency is assumed to be constant in a plasma column. We believe this understanding leads to the efficient control of the profiles of density and temperature in a helicon plasma production.

II. MODELS AND EQUATIONS

We consider a linear model composed of the equation of motion of an electron fluid neglecting the advection term (due to weak nonlinearity) and pressure gradient (almost cold plasma)

$$m_e \frac{\partial \boldsymbol{u}_e}{\partial t} = -e[\boldsymbol{E} + \boldsymbol{u}_e \times \boldsymbol{B}_0] - m_e \nu \boldsymbol{u}_e. \tag{1}$$

Faraday's and Ampere's equations

$$-\frac{\partial \boldsymbol{B}}{\partial t} = \nabla \times \boldsymbol{E}, \quad \frac{1}{c^2}\frac{\partial \boldsymbol{E}}{\partial t} + \mu_0 \boldsymbol{J} = \nabla \times \boldsymbol{B}, \tag{2}$$

with $\nabla = (\partial/\partial x, ik_y, 0)$, $\boldsymbol{J} = -en_0(x)\boldsymbol{u}_e + \boldsymbol{J}_{ext}$, and the external RF current density $\boldsymbol{J}_{ext} = I_0 \hat{z} \exp(-i\omega t)\delta(x - x_a)$. All other notations are standard. In the above, effects of the ion motion are not considered, and Cartesian coordinates are used instead of cylindrical coordinates, assuming that essential physics involved remains the same (the values of energy flux and power deposition are slightly centrally high in cylindrical coordinates compared to Cartesian coordinates in our calculation). The main axis is the x-axis (corresponding to the radial direction in the cylindrical helicon device), along which the zero-th order density is varied. Since there are no background variations in the y direction (corresponding to the axial direction in the cylindrical helicon device), all the variables are already Fourier transformed in this direction. Furthermore, the absence of nonlinear terms that may cause wave-wave interactions allows us to treat the initial k_y (the y component of the wave number) as a constant. Thus, we choose the axial mode $l_y = k_y L/\pi = 10$ excited in typical experiment[16] (the axial length of the plasma column $L = 160$ (cm) is assumed).

The above set of equations is time integrated using the standard FDTD (Finite Difference Time Domain) method. Numerical accuracy of the computation is checked by evaluating the divergence free condition of the magnetic field. Two models are considered as shown in Fig. 1. In both models, the region $0 < x < x_0$ is filled with a plasma having the background density

$$n(x) = n_{max} - (n_{max} - n_{min})(x/x_0)^2. \tag{3}$$

The adjacent region $x_0 < x < x_a$ is either a plasma with a constant density (model 1) or vacuum (model 2). At $x = x_a$, either the helicon wave (model 1) or the external RF current (model 2) is given, with the angular frequency ω satisfying

$$\omega_{ci} \ll \omega_{LH} < \omega \ll \omega_{ce} \ll \omega_{pe}, \tag{4}$$

where ω_{ci}, ω_{ce}, ω_{pe}, and $\omega_{LH} \approx (\omega_{ce}\omega_{ci})^{1/2}$ are the ion cyclotron, electron cyclotron, electron plasma, and the lower hybrid angular frequencies, respectively. The region $x > x_a$ is the wave absorber. Reflected waves are fully damped in this

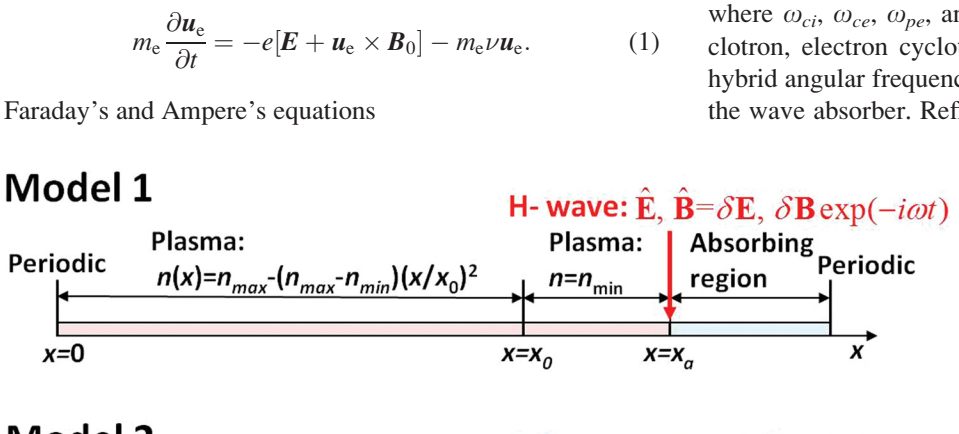

FIG. 1. Computational models used in FDTD simulation. The helicon wave propagating toward the plasma is directly excited in model 1, and the RF wave is excited by the given current in model 2.

region as shown in Fig. 1. Model 1 is employed in order to study the bulk mode conversion process. In this model, the plasma is uniform ($n = n_{\min}$) and non-dissipative ($\nu/\omega = 0$) in the region $x_0 < x < x_a$, and only the helicon wave propagating toward the plasma (H−) is directly excited at $x = x_a$. In model 2, the RF wave excited by the given current at $x = x_a$ propagates through a vacuum area and reaches the plasma. In both models, the background magnetic field B_0 is along the longitudinal (y) axis. Numerical calculations are conducted using the following typical experimental parameters: $x_0 = 7.5$ (cm), $x_a = 8.5$ (cm), $\omega/2\pi = 7.0$ (MHz), $B_0 = 0.01$ (T), electron temperature $T_e = 3.0$ (eV), Ar neutral pressure $P_{Ar} = 0.75$–10 (mTorr), $n_{\max}(0) = 4.6 \times 10^{18}[/\mathrm{m}^3]$, $n_{\min}(x_0) = 4.6 \times 10^{17}[/\mathrm{m}^3]$, and $I_0 = 1.0 \times 10^6\,[\mathrm{A/m}^2]$. Under these parameters, the MCS is located near the plasma center, and this is convenient for investigating the bulk conversion process. We note that details of the used parameters such as those specifying the boundary or the absorbing regions do not significantly alter the main conclusion of the present study. In the FDTD simulation, the electromagnetic fields are time integrated in a standard leapfrog manner, and the following boundary conditions are automatically satisfied at $x = x_0$: the tangential components of all fields and the normal component of **B** field are continuous. Numerical iterations are conducted using the following parameters: grid size $dx = 6.0 \times 10^{-5}$[m], time step $dt = 0.9dx/c$[s], number of grids in the plasma region ($0 < x < x_0$): 1250, number of grids in the vacuum region ($x_0 < x < x_a$): 166, number of grids in the absorbing region ($x_a < x$): 500, and the typical number of time steps for a single run: 2.4×10^6 ($\approx 3.0 \times 2\pi/\omega$).

We assume that the electron-neutral collision is dominant, and this allows us to replace the collision frequency in (1) by the electron-neutral collision frequency, $\nu = \nu_{en}$, which is given approximately by[16]

$$\nu_{en}[\mathrm{sec}^{-1}] \approx 1.3 \times 10^6\, P_{Ar}[\mathrm{mTorr}]\, T_e[\mathrm{eV}], \tag{5}$$

and thus the electron-neutral collision frequency is within the range $\nu/\omega \approx 0.067 \sim 0.89$.

After a transient time period ($t > 3.0 \times 2\pi/\omega_{rf}$), the magnetic field perturbations satisfy a set of equations derived by Fourier transforming (1) and (2) in t

$$B_x' = -ik_y B_y, \tag{6}$$

$$B_y'' = -ik_y\left(\frac{n'}{n}B_x - B_x'\right) + \frac{\omega_{pe}^2}{c^2\gamma}B_y + \frac{n'}{n}B_y' - \frac{\omega_{ce}k_y}{\omega\gamma}\left(\frac{n'}{n}B_z - B_z'\right), \tag{7}$$

$$B_z'' = i\frac{\omega_{ce}}{\omega\gamma}k_y^2 B_x - \frac{\omega_{ce}}{\omega\gamma}k_y B_y' + \left(\frac{\omega_{pe}^2}{c^2\gamma} + k_y^2\right)B_z + \frac{n'}{n}B_z', \tag{8}$$

where $\gamma = 1 + i(\nu/\omega)$ and $'$ denotes d/dx. The boundary value problem at the plasma region ($0 < x < x_0$) defined by (6)–(8) is solved using the fourth-order Runge Kutta method. The values at the boundaries are given at the plasma center ($x = 0$) as follows:

$$(B_x\, B_y\, B_z\, B_y'\, B_z')_{x=0} = (B_{x,H-}\, B_{y,H-}\, B_{z,H-}\, B_{y,H-}'\, B_{z,H-}')_{x=0},$$

where the subscript H− denotes the H− mode. The relative values of each component are determined by the dispersion relation with the density at the plasma center $n(0)$. Variables at the plasma edge ($x = x_0$) are to be determined after integration of (6)–(8). Since the boundary value problem above and also the FDTD simulation system are both linear, waves included in these systems can be decomposed into the combination of the four modes (H+, TG+, H−, TG−), i.e., the helicon (H) and the TG waves propagating both in the positive (+) and the negative (−) directions with respect to the x-axis.

The decomposition can be carried out by solving the dispersion relation at each location assuming validity of the WKB approximation. The zeroth-order condition to apply the WKB method is given by the factor[19]

$$f_{WKB} = \left|\frac{1}{k_x^2}\frac{dk_x}{dx}\right|. \tag{9}$$

Figure 2 shows f_{WKB} for the helicon and the TG waves for $\nu/\omega = 0.003$ and 0.005. We see that $f_{WKB} < 1$ for the entire space for the TG wave and near the center of the plasma including the MCS for the helicon wave. We should also note that f_{WKB} is not much less than unity near the MCS, and it exceeds unity for the helicon wave for $x > 0.04$ (m). Therefore, the WKB decomposition is approximately valid (but not exact) near the center of the plasma including the MCS, since the gradient scale of the background is less than the helicon wavelength near the plasma edge. Here, we wish to stress that our solutions of the boundary value problem and the FDTD simulations are correct, within the accuracy of numerical errors and using discrete grids with a finite width.

III. RESULTS AND DISCUSSIONS

A. Dispersion relation

Solving the Fourier transformed equations of (1) and (2) with respect to k_x, one can obtain the bi-quadratic equation and find its roots in the following form:

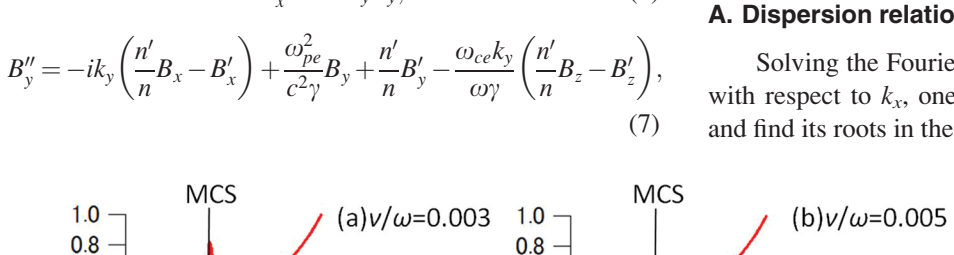

FIG. 2. f_{WKB} profiles of the helicon (red) and the TG (blue) waves for $\nu/\omega =$ (a) 0.003 and (b) 0.005.

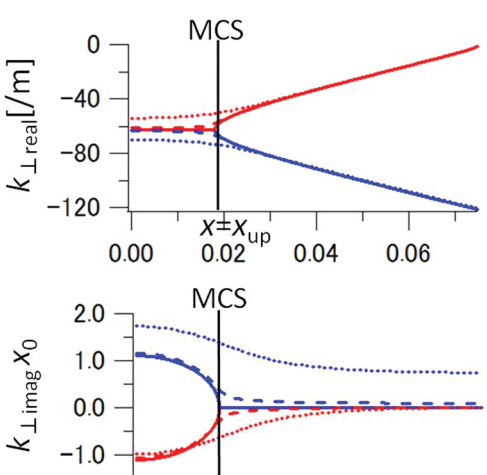

FIG. 3. Dispersion relation of the H− wave (red) and the TG+ wave (blue), with $\nu/\omega = 0$ (solid), 0.01 (dashed), and 0.08 (dotted).

$$k_{x\pm}^2 = k_y^2 \frac{1}{2\gamma^2\alpha^2\beta^2}\left(1 - 2\gamma\alpha - 2\gamma^2\alpha^2\beta^2 \pm \sqrt{1 - 4\gamma\alpha}\right), \quad (10)$$

where

$$\alpha = \frac{\omega_{pe}^2\omega^2}{\omega_{ce}^2 c^2 k_y^2} \quad \text{and} \quad \beta = \frac{\omega_{ce} c^2 k_y^2}{\omega_{pe}^2 \omega}. \quad (11)$$

Two different waves can be seen from (10), the minus sign corresponds to the helicon wave, and the plus sign corresponds to the TG wave. Figure 3 shows dispersion relations of the H− (red lines) and TG+ waves (blue lines), where the minus sign represents the sign of the wave phase velocity (note that the perpendicular component of the TG wave group velocity has an opposite sign to that of the phase velocity). Dispersion curves with $\nu/\omega = 0$ (solid lines), 0.01 (dashed), and 0.08 (dotted) are superposed. The upper panel shows the real wave number. When the collision is absent, dispersion curves of H− and TG+ merge at $x = x_{\mathrm{up}}$, corresponding to the MCS where the discriminant in (10) is zero, and the H− mode converts to the TG+ as the reflected wave. When a finite collision is added, the dispersion curves are separated because the discriminant in (10) includes the imaginary part and cannot be zero (the same discussion holds for the case with including the effect of strong density gradient[10] in (10)). The separation is increased as ν/ω is increased, reducing efficiency of the mode conversion between the H− and TG+ waves. The bottom panel of Fig. 3 shows the normalized imaginary wave number, $k_{\perp\mathrm{imag}}x_0$, showing the reciprocal of damping scale normalized to the size of the plasma column. When $\nu/\omega \neq 0$, $k_{\perp\mathrm{imag}}x_0 \ll 1$ in the low density region. As the H− wave propagates toward the center where the density is increased, $k_{\perp\mathrm{imag}}x_0$ becomes larger, and the wave penetrates into the evanescent region ($x > x_{\mathrm{up}}$).

B. Wave and energy flux profiles

Now, we discuss the bulk mode conversion by using model 1. Figure 4 shows a typical result of numerical time integration of (1) and (2) by solid lines. Initially, there is no perturbation field in the system, and the H− wave is introduced at $x = x_a = 8.5$ (cm). Plotted in (a) and (c) are the real parts of wave magnetic field, $\mathrm{Re}[B_z]$, of H− (red lines) and TG+ (blue lines) waves at $t = 3.4 \times 2\pi/\omega_{\mathrm{rf}}$, with $\nu/\omega = 0$ in (a) and $\nu/\omega = 0.02$ in (c). Numerical solutions of (6)–(8) are also shown as dotted lines. In model 1, almost no H+ and TG− waves are excited because only the H− wave is excited in this model. Sharp peaks of the magnetic perturbations around $x = x_{\mathrm{up}}$ in (a) are due to the degeneracy of H− and TG+ waves: the perturbation field cannot be decomposed into the four wave modes when the waves are degenerated. The total field perturbation has no singular behavior. Figures 4(b) and 4(d) show the computed x-component of the energy flux in the boundary value problem (Eqs. (6)–(8)) and the FDTD simulation, $\Gamma_{x,\mathrm{H-}} = \mathrm{Re}[\boldsymbol{E}_{\mathrm{H-}} \times \boldsymbol{B}^*_{\mathrm{H-}}]_x/\mu_0$, for the H− ($\Gamma_{x,\mathrm{H-}} < 0$) waves, and $\Gamma_{x,\mathrm{TG+}} = \mathrm{Re}[\boldsymbol{E}_{\mathrm{TG+}} \times \boldsymbol{B}^*_{\mathrm{TG+}}]_x/\mu_0$, for the TG+ ($\Gamma_{x,\mathrm{TG+}} > 0$) waves (the Poynting flux also involves terms such as $\mathrm{Re}[\boldsymbol{E}_{\mathrm{H-}} \times \boldsymbol{B}^*_{\mathrm{TG+}}]_x/\mu_0$, but due to the difference in the wavenumbers for different wave modes, the direction of the cross product oscillates in space and they do not contribute much in conveying the energy flux over the entire plasma region). When $\nu/\omega = 0$, waves become evanescent at $x = x_{\mathrm{up}}$, and total Γ_x vanishes because the energy

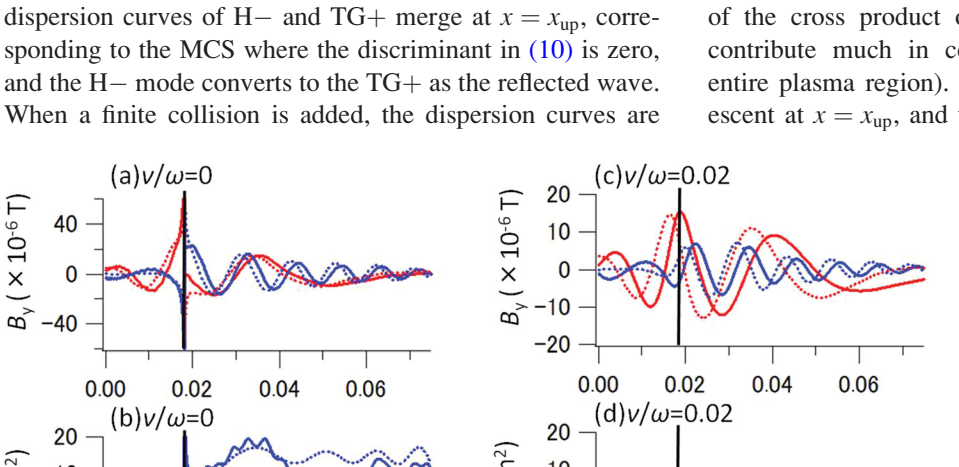

FIG. 4. Wave fields: $\mathrm{Re}[B_z]$ (top), and x components of energy flux: Γ_x (bottom) at $t = 3.4 \times 2\pi/\omega_{\mathrm{rf}}$, with the H− wave (red line) and the TG+ wave (blue line), FDTD simulation (solid line) and numerical analytical solutions (dotted line) of (6)–(8).

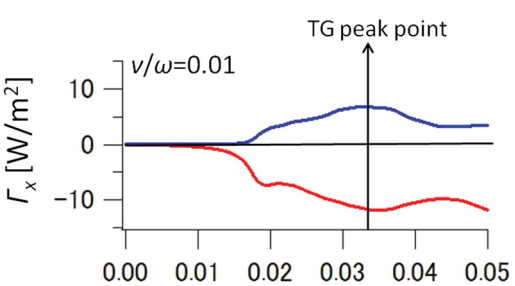

FIG. 5. The energy flux profiles of the helicon (red) and the TG waves (blue). Λ is evaluated at the point where the TG energy flux is maximum.

fluxes carried into the plasma are all reflected. In particular, we see in (b) that the energy flux conveyed by H− is all converted to that of TG+. The electromagnetic field perturbations penetrate into the evanescent region ($x > x_{up}$), but there is no energy flux associated with the perturbations. When $\nu/\omega = 0.2$, the balance of energy flux does not hold due to the wave dissipation, and the total Γ_x does not vanish. The wave amplitude of TG+ in this case is considerably smaller than the collision-less case. The decrease of the transformed energy by the bulk mode conversion is due to the separation of the helicon and the TG wave branches in the dispersion relation. The energy flux of helicon wave flows into bulk area ($x > x_{up}$), and the helicon wave directly decays near the MCS ($x \approx x_{up}$) because $k_{\perp imag} x_0$ becomes larger (Fig. 3). However, the bulk mode conversion is still visible in this case $\nu/\omega = 0.02$.

C. Bulk mode conversion efficiency

The efficiency of TG wave excited by the bulk mode conversion strongly depends on the dissipation as stated above. Here, we evaluate the efficiency as a function of the dissipation parameter. We define the mode conversion efficiency as $\Lambda = \Gamma_{x,TG+}/\Gamma_{x,H-}$. Figure 5 compares the energy flux carried by the H− and TG+ waves for $\nu/\omega = 0.01$. The MCS is located near $x = 0.02$. Due to the uncertainty of the location of the mode conversion, it is difficult to evaluate Λ exactly. Here, we identify the point where the TG energy flux is maximum and compute Λ at this point. Table I and Fig. 6 show the dependence of Λ on ν/ω. $\Gamma_{x,H-}$, $\Gamma_{x,TG+}$, and Λ are evaluated by both FDTD simulation and numerical solutions of (6)–(8) as shown in Table I (numerical results of $\Gamma_{x,H-}$ and $\Gamma_{x,TG+}$ are not listed).

TABLE I. The evaluated energy fluxes of the helicon and the TG waves, and the computed mode conversion efficiency.

ν/ω	$\Gamma_{x,H-}$ (W/m²) Simulation	$\Gamma_{x,TG+}$ (W/m²) Simulation	Λ (%) Simulation	Λ (%) Analysis
0	−29.81	29.12	98	100
0.003	−29.17	29.73	95	81
0.005	−27.79	23.71	85	71
0.008	−26.51	16.67	63	60
0.01	−25.55	13.34	52	52
0.02	−21.24	4.82	23	28
0.03	−18.20	1.98	11	16
0.04	−16.12	0.90	6	9
0.05	−14.71	0.45	3	6
0.06	−13.80	0.24	2	4

As ν/ω is increased, Λ decreases monotonically. In particular, Λ is almost 100% when $\nu/\omega = 0$, Λ remains above 50% when $\nu/\omega < 0.01$, and $\Lambda < 10\%$ when $\nu/\omega > 0.04$, corresponding to usual laboratory experiments (assuming no neutral depletion). The bulk mode conversion is important only when the dissipation is small.

D. Power deposition

Finally, we discuss the power deposition (local joule heating) profiles of the four modes, P_{abs}, by using model 2

$$P_{\rm abs}(x) = {\rm Re}[\boldsymbol{E}\cdot\boldsymbol{J}] = \frac{\omega\varepsilon_0}{2}{\rm Im}\left\{S\left(|E_x|^2+|E_z|^2\right)+P|E_y|^2\right\}, \quad (12)$$

where S and P are the notations used in Stix.[23] Figure 7 compares $P_{\rm abs}$ of the four wave modes for various values of ν/ω. When (a) $\nu/\omega = 0.003$, the power deposition profiles exhibit sharp peaks near the MCS, indicating an abrupt change of the damping scale length near the MCS (see the bottom panel of Fig. 3). The power deposition of the TG+ wave excited by the bulk mode conversion is comparable to that of the TG− wave excited by the surface mode conversion. The power absorption by the H+ wave is very small. This is due to the reverse bulk mode conversion, i.e., the energy transfer occurs from TG− to H+. When (b) $\nu/\omega = 0.02$, the power deposition by the bulk mode conversion decreases but is still comparable to that of the surface mode conversion, and the power deposition of the H− wave becomes dominant. The H− wave mainly heats the bulk region, while the TG+ and TG− waves heat the plasma over an extended region. Under typical experimental conditions ((c) $\nu/\omega = 0.07$ and (d) 0.8), the bulk mode conversion cannot be seen and the H− wave is directly damped over the extended region. The power deposition is comparable to that of the TG+ wave. Our results here are quite different from conventional analysis of the collisional power absorption where the analysis was made only at locations far from the MCS. The power deposition of the TG+ wave becomes more dominant and localized at the edge ($x \approx x_0$) as ν/ω is increased. Actually, the energy of the TG− wave, excited by the surface mode conversion, depends on the edge density (increases as the edge density increases,

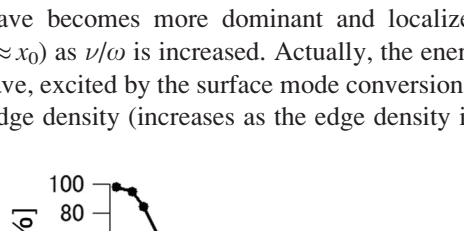

FIG. 6. The dependence of computed mode conversion efficiency (from the H− wave to the TG+ wave) Λ in the FDTD simulation, on the normalized collision frequency, ν/ω.

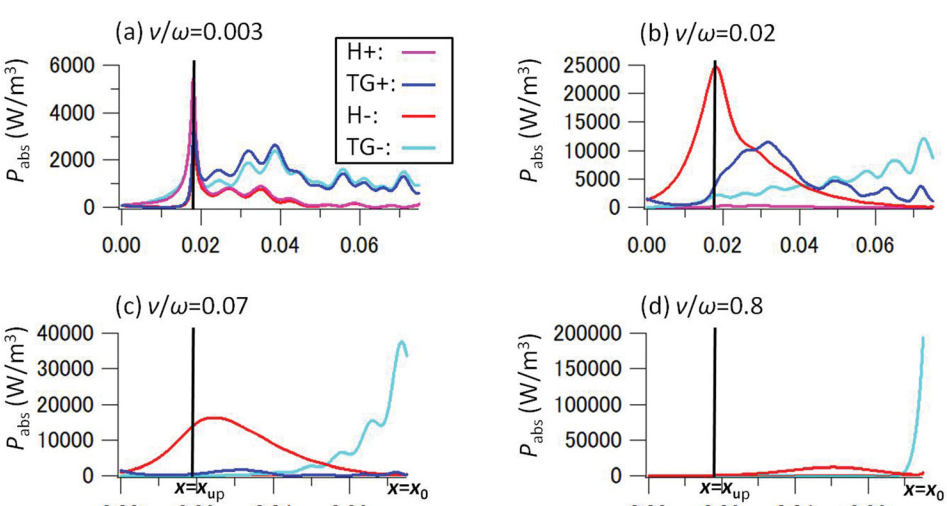

FIG. 7. Power deposition profiles of the four modes (H+, TG+, H−, TG−) for $\nu/\omega =$ (a) 0.003, (b) 0.02, (c) 0.07, and (d) 0.8.

and vise versa). Therefore, the relative importance of the heating by each wave also depends on the edge density.

IV. CONCLUSION

We have clarified the contribution of the bulk mode conversion and the helicon wave for the power deposition under typical experimental conditions: the efficiency of the bulk mode conversion strongly depends on the collision frequency. We also investigated the power deposition profiles due to the four modes (H+, TG+, H−, TG−) varying the collision frequency. In conclusion, the structure of the power deposition can be roughly classified into the following cases:

Case 1: Small collision frequency ($\nu/\omega < 0.01$): Highly efficient bulk mode conversion occurs. The TG waves are excited by the bulk mode conversion, and the surface mode conversion plays crucial roles in the plasma heating. Power deposition is maximized near the MCS for all the wave modes.

Case 2: Moderate collision frequency ($0.01 < \nu/\omega < 0.06$): The bulk mode conversion is not as evident as in case 1 but is still important for the power deposition as the surface mode conversion. The central heating by the helicon wave is most dominant.

Case 3: Large collision frequency ($0.06 < \nu/\omega$): This is the case for typical laboratory experiments. The bulk mode conversion is not dominant. The input helicon wave energy directly dissipates and heats the plasma. The power deposition of the TG wave excited by the surface mode conversion becomes more dominant at the plasma edge as the collision frequency increases.

The bulk mode conversion and the bulk helicon heating are important only when the collision frequency is small (cases 1 and 2). However, when the plasma density is high, significant plasma heating may trigger the development of a neutral depletion in an actual helicon discharge, and the bulk mode conversion and the bulk helicon heating may become important. Therefore, further arguments of the helicon power deposition should include a non-uniform distribution of the collision frequency due to the neutral depletion and the plasma heating.

[1]F. F. Chen, Plasma Sources Sci. Technol. **24**, 014001 (2015).
[2]F. F. Chen, Plasmas Phys. Controlled Fusion **33**, 339 (1991).
[3]F. F. Chen and D. D. Blackwell, Phys. Rev. Lett. **82**, 2677 (1999).
[4]D. D. Blackwell and F. F. Chen, Plasma Sources Sci. Technol. **10**, 226 (2001).
[5]A. I. Akhiezer, V. S. Mikhailenko, and K. N. Stepanov, Phys. Lett. A **245**, 117 (1998).
[6]J. L. Kline and E. E. Scime, Phys. Plasmas **10**, 135 (2003).
[7]B. Lorenz, M. Krämer, V. L. Selenin, and Yu. M. Aliev, Plasma Sources Sci. Technol. **14**, 623 (2003).
[8]K. P. Shamrai, Plasma Phys. Controlled Fusion **36**, 635 (1994).
[9]K. P. Shamrai, Plasma Sources Sci. Technol. **7**, 499 (1998).
[10]Yu. M. Aliev and M. Krämer, Phys. Plasmas **15**, 104502 (2008).
[11]F. F. Chen and D. Arnush, Phys. Plasmas **4**, 3411 (1997).
[12]Y. Mouzouris and J. E. Scharer, Phys. Plasmas **5**, 4253 (1998).
[13]D. Arnush, Phys. Plasmas **7**, 3042 (2000).
[14]D. D. Blackwell, T. G. Madziwa, D. Arnush, and F. F. Chen, Phys. Rev. Lett. **88**, 145002 (2002).
[15]S. Shinohara and K. P. Shamrai, Plasma Phys. Controlled Fusion **42**, 865 (2000).
[16]K. P. Shamrai and S. Shinohara, Phys. Plasmas **8**, 4659 (2001).
[17]V. F. Virko, G. S. Kirichenko, and K. P. Shamrai, Plasma Sources Sci. Technol. **11**, 10 (2002).
[18]D. Arnush and F. F. Chen, Phys. Plasmas **5**, 1239 (1998).
[19]S. H. Kim and Y. S. Hwang, Plasma Phys. Controlled Fusion **50**, 035007 (2008).
[20]A. Fruchtman, G. Makrinich, P. Chabert, and J. M. Rax, Phys. Rev. Lett. **95**, 115002 (2005).
[21]J. L. Raimbault, L. Liard, J. M. Rax, P. Chabert, A. Fruchman, and G. Makrinich, Phys. Plasmas **14**, 013503 (2007).
[22]R. M. Magee, M. E. Galante, J. Carr, Jr., G. Lusk, D. W. McCarren, and E. E. Scime, Phys. Plasmas **20**, 123511 (2013).
[23]S. H. Stix, *Theory of Plasma Waves* (Wiley, New York, 1962).